Editors' Suggestion

Three-Dimensional Active Defect Loops

Jack Binysh,[1] Žiga Kos,[2] Simon Čopar,[2] Miha Ravnik,[2,3,*] and Gareth P. Alexander[4,†]
[1]*Mathematics Institute, Zeeman Building, University of Warwick, Coventry CV4 7AL, United Kingdom*
[2]*Faculty of Mathematics and Physics, University of Ljubljana, Jadranska 19, 1000 Ljubljana, Slovenia*
[3]*Jožef Stefan Institute, Jamova 39, 1000 Ljubljana, Slovenia*
[4]*Department of Physics and Centre for Complexity Science, University of Warwick, Coventry CV4 7AL, United Kingdom*

(Received 16 September 2019; accepted 23 January 2020; published 25 February 2020)

We describe the flows and morphological dynamics of topological defect lines and loops in three-dimensional active nematics and show, using theory and numerical modeling, that they are governed by the local profile of the orientational order surrounding the defects. Analyzing a continuous span of defect loop profiles, ranging from radial and tangential twist to wedge $\pm 1/2$ profiles, we show that the distinct geometries can drive material flow perpendicular or along the local defect loop segment, whose variation around a closed loop can lead to net loop motion, elongation, or compression of shape, or buckling of the loops. We demonstrate a correlation between local curvature and the local orientational profile of the defect loop, indicating dynamic coupling between geometry and topology. To address the general formation of defect loops in three dimensions, we show their creation via bend instability from different initial elastic distortions.

DOI: 10.1103/PhysRevLett.124.088001

Active matter is a class of materials in which the individual constituents continually consume energy to generate work or motion, maintaining the system in dynamic, self-organized, nonequilibrium states [1,2]. Examples derive readily from the study of living systems, ranging from intracellular organization to swarming bacteria and flocks of birds, but they can equally be realized synthetically in self-propelled colloids or microtubule mixtures. The formalism of active liquid crystals [3] has emphasized the key role of topology in active matter, showing the significance of active topological defects to "turbulence" in bacterial suspensions [4], cell populations [5], cultures [6], and tissues [7], as well as synthetic active nematics [8,9]. Central to much of the phenomenology in (quasi-) two-dimensional systems is that defects with a $+1/2$ profile actively self-propel, while those with $-1/2$ profile do not [10].

The major focus to date has been on topological defects in two-dimensional active systems [11–14], including in curved geometries [9,15–17]; however, recently results have begun to emerge also in three dimensions. Three-dimensional active nematics are governed by the presence of topological defect lines and loops, which exhibit complex structure and topology-affected dynamics. These have been studied numerically in thin slabs [18], establishing the crossover from two-dimensional behavior and the significance of twist distortions, and in the confined geometry of a spherical droplet [19], showing the significance of defect loops in the turbulent regime. Recent experiments in a bulk extensile nematic [20] confirm the importance of defect loops, particularly those of zero topological charge, and provide insights into their structure, formation, and dynamics.

Active nematics are described by a local orientation $\mathbf{n}$, called the director, which is a unit line field satisfying the symmetry $\mathbf{n} \sim -\mathbf{n}$, and active stresses $-\zeta \mathbf{nn}$ along this orientation [1], where ζ is a phenomenological constant that is positive in extensile materials and negative in contractile ones. Defects are regions where the local orientation of the active nematic is broken due to frustration and in three dimensions are, usually, in the form of lines, which can close into loops. The geometric structure of a defect line is encoded in its profile, the variation of the director field in a perpendicular cross section. In the two-dimensional $\pm 1/2$ profiles the director lies in this cross-sectional plane; however, in three dimensions a far greater range of geometric profiles is possible [19–26]. The topological classification of nematic defect loops is also rich, particularly the interplay between topological charge and orientability [21–23].

In this Letter, we describe the three-dimensional flows generated by active defect lines and zero topological charge defect loops, applicable to systems such as microtubule-based active nematics [8,20]. Using analytic calculations and mesoscopic continuum numerical modeling, we show that the nonlinear dynamics of three-dimensional active

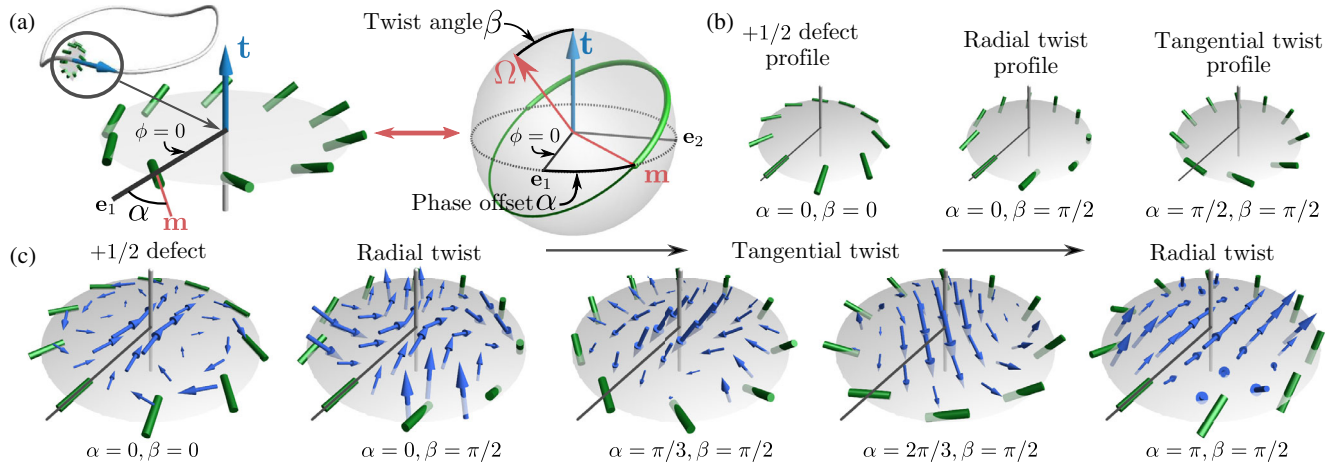

FIG. 1. Three-dimensional local profiles of defect lines and their flows. (a) A local director profile (green cylinders) corresponds to a path on the unit sphere connecting antipodal points. We consider minimal distortion profiles corresponding to half a great circle (thickened green line)—these are specified by a twist angle β and a phase offset angle α. (b) Selected examples of defect profiles of $+1/2$ and "pure twist" type. (c) The active flows (blue arrows) generated by the corresponding nematic defect profiles. We show the case of extensile activity ($\zeta > 0$); for contractile activity the direction of the flows reverses.

nematic defects can be understood in terms of their local director profile and associated "self-propulsion velocity." We then give a statistical analysis of the geometries of defect loops in three-dimensional active turbulence in the confinement of a sphere, showing that the most common profiles are of twist type and that $\pm 1/2$ profiles occur preferentially at places of high curvature. Finally, we describe the process of defect loop formation from the uniform state via the fundamental bend instability of extensile nematics.

If we plot the variation of the director around any cross section of a defect line as a path on the unit sphere it traces out a curve connecting antipodal points, Fig. 1(a). We restrict to those profiles for which this curve is half of a great circle; the rotation of the director around the defect line is then as efficient as possible, which minimizes the total elastic distortion. Since any (oriented) great circle can be identified with the vector $\mathbf{\Omega}$ normal to it, the space of these minimal distortion profiles is S^2; defect loops of this type, described by the rotation vector $\mathbf{\Omega}$, were first introduced by Friedel and de Gennes [24]. We parametrize this space as follows: Let $\mathbf{t}$ denote the unit tangent to the defect line. Any great circle is orthogonal to $\mathbf{t}$ either at exactly two points, $\pm\mathbf{m}$, or at every point; the latter are the $\pm 1/2$ profiles of defects in two-dimensional active nematics. We take the defect profile to be the half great circle starting at $\mathbf{m}$ and ending at $-\mathbf{m}$ with director

$$\mathbf{n} = \cos\frac{1}{2}\phi\mathbf{m} + \sin\frac{1}{2}\phi(\cos\beta\mathbf{t}\times\mathbf{m} + \sin\beta\mathbf{t}), \quad (1)$$

where ϕ is the azimuthal angle about the defect line and β is the "twist angle" between $\mathbf{t}$ and $\mathbf{\Omega}$. The profile is called "wedge type" ($\pm 1/2$) if $\beta = 0$, π and "twist type" if $\beta = \pi/2$ [20]; we caution that the word twist here does not hold direct correspondence with a specific type of elastic distortion. We denote by α the "phase offset" between $\mathbf{m}$ and the direction $\mathbf{e}_1$ of the radial line $\phi = 0$, and write $\mathbf{m} = \cos\alpha\mathbf{e}_1 + \sin\alpha\mathbf{e}_2$, where $\mathbf{e}_2 = \mathbf{t}\times\mathbf{e}_1$. Distinct examples of how the phase offset affects the local geometry of twist profiles are given by the cases $\alpha = 0$, π (radial twist) and $\alpha = \pm\pi/2$ (tangential twist), as shown in Fig. 1(b). We remark that this parametrization is not unique; e.g., under the nematic symmetry $\mathbf{n}\to-\mathbf{n}$ we have $(\alpha,\beta)\to(\alpha+\pi,-\beta)$.

To determine the nature of the active flows generated by three-dimensional defect lines we adapt the approach of Giomi *et al.* [10] for defects in two dimensions. The idea is to solve a Stokes flow problem for an incompressible fluid

$$-\nabla p + \mu\nabla^2\mathbf{u} - \zeta\nabla\cdot(\mathbf{nn}) = 0, \qquad \nabla\cdot\mathbf{u} = 0, \quad (2)$$

with an active forcing term $-\zeta\nabla\cdot(\mathbf{nn})$ and prescribed director field Eq. (1). The solution is obtained by taking a Helmholtz decomposition of the active force [27]; we present this in the Supplemental Material [28] and show examples in Fig. 1(c), focusing on a family interpolating between profiles of radial and tangential twist. By evaluating the flow at the location of the defect itself we obtain a self-propulsion velocity,

$$\mathbf{u}_{\mathrm{SP}} = -\frac{\zeta R_\perp(1+\cos\beta)^2}{16\mu}(\cos 2\alpha\mathbf{e}_1 + \sin 2\alpha\mathbf{e}_2) - \frac{\zeta R_\parallel\sin\beta(1+\cos\beta)}{4\mu}\sin\alpha\mathbf{t}, \quad (3)$$

where $R_\perp$, $R_\parallel$ are length scales roughly corresponding to the typical defect spacing, or the (local) radius of curvature of the defect loop. More formally, they are constants of integration arising from the choice of boundary conditions in exactly the same way as in the calculation for defects in two dimensions [10]. This result has several immediate interesting aspects. First, the magnitude of the transverse velocity depends only on β while its direction is determined by $\mathbf{m}$ and rotates relative to the radial direction $\phi = 0$ at the rate 2α. Second, generically there is also a component of motion (and flow) directed along the defect line; it has maximum strength when $\alpha = \pm\pi/2$ and $\beta = \pm\pi/3$ and vanishes only at profiles with $\alpha = 0, \pi$, or $\beta = \pi$. These tangential flows locally stretch the defect line creating elongated sections of loops with such profiles. Third, the self-propulsion velocity vanishes entirely only when $\beta = \pi$, corresponding to the $-1/2$ profile.

This calculation qualitatively predicts the behavior of three-dimensional active defect loops by assigning, at each point, a local profile given by Eq. (1) and the corresponding self-propulsion velocity Eq. (3). In doing this we neglect contributions coming from the curvature of the defect loop but capture the important leading behavior of self-propulsion. Figure 2 shows analytical results (top panels) and full numerical simulations (middle and bottom panels) of active flows and dynamics for three distinct types of defect loop with zero topological charge, initiated as surrounding cylindrical domains of either a splay, bend, or twist elastic distortion; these loop types directly correspond to those identified in recent experiments [20]. In each case, we consider a slab geometry, confined along z and periodic in x, y, and initialize a circular defect loop in the cell midplane, working in the regime of weak activity below the threshold for onset of spontaneous flows [29,30]. The director field around a defect loop with arbitrary geometry (and topology) can be created using Maxwell's solid angle function; as this function is harmonic, this creates director fields that satisfy the (one-elastic-constant) Euler-Lagrange equations [24,31,32]. Details of numerical methods and parameter values are given in the Supplemental Material [28], which includes Refs. [30,33].

We show in Fig. 2(a) a defect loop surrounding a splay domain, with the director uniformly along z outside the loop and matching to normal anchoring at both boundaries. Inside the defect loop the director rotates to point along x in the cell midplane, giving a splay distortion there. A full mapping of the local profiles along the defect loop to Eq. (1) is given in the Supplemental Material [28], but it suffices to focus on only a few points. In the xz-plane the local profile is $+1/2$ at positive x and $-1/2$ at negative x; the associated active flows cause the $+1/2$ point to propel along positive x, while the $-1/2$ point does not intrinsically self-propel. In the yz-plane the profile is of tangential twist type with $\beta = \pi/2$, $\alpha = \pm\pi/2$ and at both points the

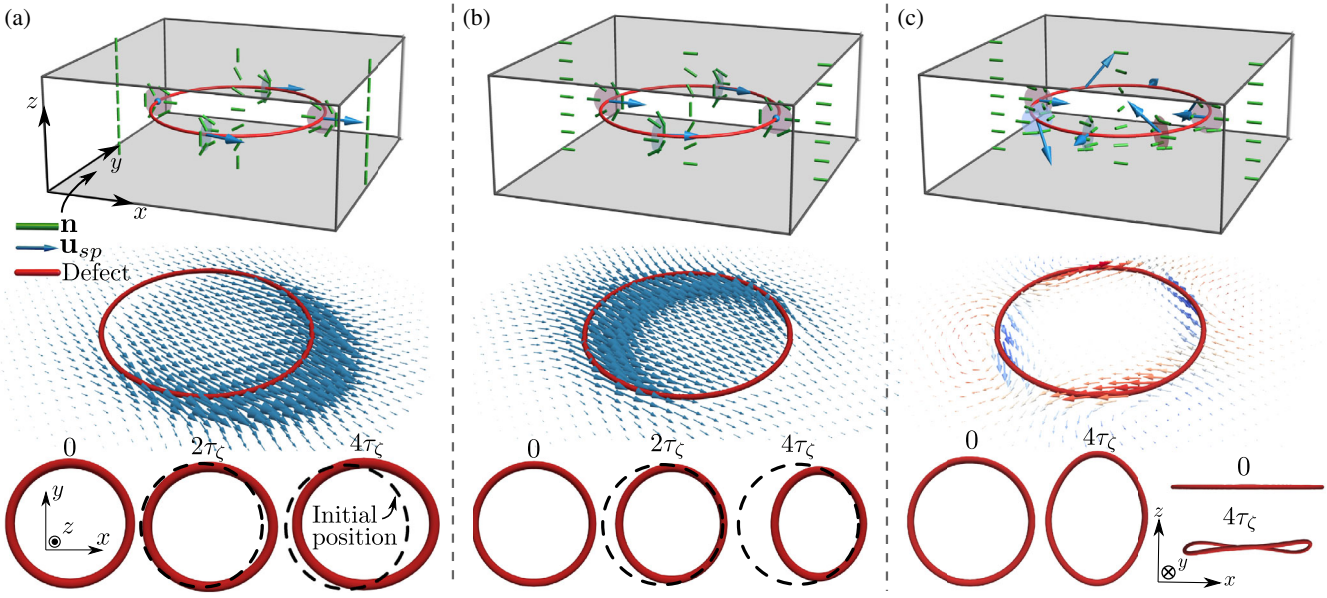

FIG. 2. Flows and dynamics of different active nematic defect loops with zero topological charge. (a) Defect loop surrounding a cylindrical splay domain (director shown in green). The top panel shows a schematic with the analytically predicted self-propulsion velocity (blue arrows), the middle panel shows the numerically calculated flows in the cell midplane, and the bottom panel shows the dynamics of the defect loop position and shape. (b) Defect loop surrounding a cylindrical bend domain with the same comparison between analytic predictions and full simulation as in (a). (c) Defect loop surrounding a cylindrical twist domain. Here the profile is of twist type ($\beta = \pi/2$) everywhere and α makes two full rotations around the loop. The self-propulsion velocities contract the loop along x, expand it along y, and buckle it on its diagonals. Color on the middle panel velocity gives its z component ($+z$ red, $-z$ blue). Time in all panels is given in units of the active timescale τ_ζ (see Supplemental Material [28]).

tangential component of the flow is along positive x, stretching these sections. Putting these local pieces together, the defect loop self-propels along positive x and expands into a prolate shape as it does so. This prediction is in remarkably close qualitative agreement with numerical solutions for the velocity field and loop evolution from the full active nematic equations for the velocity.

Switching to planar alignment along the x-direction with the director vertical inside the defect loop generates a loop surrounding a bend domain, shown in Fig. 2(b). Here, in the xz-plane, we have a $+1/2$ defect at negative x, a $-1/2$ defect at positive x, and tangential twist profiles with $\beta = \pi/2$, $\alpha = \pm\pi/2$ in the yz-plane. This leads to the loop self-propelling along positive x, this time shrinking and adopting an oblate shape.

The behavior is different for a defect loop surrounding a (right-handed) twist domain, shown in Fig. 2(c). The director rotates within the xy-plane of the cell so that every cross-sectional profile is of pure twist type, with $\beta = \pi/2$ in Eq. (1). For such a defect loop, the transverse component of the self-propulsion velocity has constant magnitude and winds around the defect loop with linking number -2 (see Supplemental Material [28]); its direction is such as to compress the loop along the x-axis and expand it along y, to push it down at points lying along the $x = y$ diagonal and up at points on the $x = -y$ diagonal. The net effect is to cause the defect loop to buckle into a nonplanar shape (the sense of buckling reverses upon reversal of the twist domain handedness).

We investigate what the local profile structure along an active defect loop typically is, using simulations of the turbulent state in a spherical droplet where loops are continually produced, annihilated, and rewired [19]. The local profiles of all defect loops are extracted and tracked dynamically over the simulation time (see Supplemental Material [28] for details of the extraction algorithm, which includes Refs. [34,35]). Figure 3(a) shows a typical simulation snapshot in which there are three defect loops and the profiles of each. Because of the spherical confinement, one of the loops has $+1$ topological charge while the others have zero charge; in the following we consider only the zero topological charge loops.

In Fig. 3(b) we plot the distribution of local profiles found over the entire simulation using an equal-area projection of the (α, β) sphere [Fig. 1(a)]. The distribution shows a bias towards profiles of twist type ($\beta \approx \pi/2$) with tangential twist ($\alpha \approx \pm\pi/2$) more common than radial twist ($\alpha \approx 0, \pi$). We speculate that this bias is caused by the flows about tangential twist profiles locally stretching the defect line, as discussed for Fig. 2(a), increasing the length of the loop with this local profile. We also note a symmetry between (α, β) and $(-\alpha, \beta)$, a consequence of invariance under $\mathbf{t} \to -\mathbf{t}$ coming from the fact that the defect loops are not naturally oriented, but a slight asymmetry between

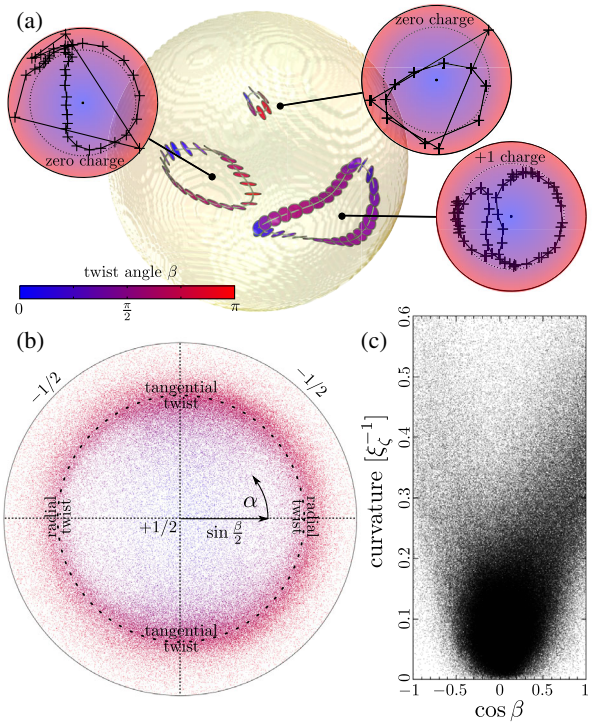

FIG. 3. Statistics of defect loop profiles. (a) Typical snapshot of a spherical droplet in the turbulent regime, showing three defect loops with cross sections colored by twist angle β. Insets show the variation of profiles for each loop in an equal-area projection of the (α, β) sphere. (b) Cumulative statistics of defect loop profiles (zero topological charge loops only). The majority are of twist type ($\beta \approx \pi/2$), with a maximum at tangential twist profiles ($\alpha \approx \pm\pi/2$). (c) Correlation between local defect line curvature and twist angle β (units are inverse active length scale ξ_ζ^{-1}; see Supplemental Material [28]).

(α, β) and $(\alpha + \pi, \beta)$. This asymmetry is detecting the global structure of flows confined to a droplet, which spontaneously pick an axis and sense of rotation, as detailed in [19]. Finally, in Fig. 3(c) we plot the twist angle β against the local defect line curvature, which shows that the twist profiles ($\cos\beta \approx 0$) coincide with the places of lowest curvature, while the wedge-type $\pm 1/2$ profiles reside at "apex points" where the curvature is highest. This correlation is consistent with the dynamics of the highly idealized loop encircling a splay domain, shown in Fig. 2(a), and the formation of hairpins under the combination of transverse self-propulsion of $+1/2$ points and line stretching of tangential twist profiles.

Defect loops in three-dimensional active nematics can nucleate directly from bend instability, in direct analogy with the nucleation of $\pm 1/2$ point defect pairs in two dimensions [8,36]. To study this important nucleation process, we initialize a localized bend distortion in a homogeneous far field director; see Fig. 4(a). The bend distortion grows until it nucleates a defect loop in the cell midplane, whose structure is exactly that of the defect

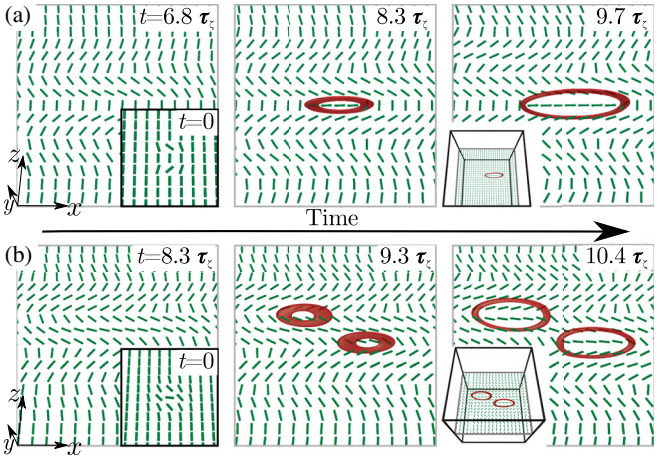

FIG. 4. Nucleation of zero topological charge active nematic defect loops. (a) A localized bend distortion in the director (inset, green) seeds a defect loop (red) via the generic bend instability. The nucleated loop has the same structure as that surrounding the splay domain shown in Fig. 2(a). (b) Seeds of different elastic distortions generate defect loops of the same type, emerging from regions of maximal bend by the same generic instability.

loop surrounding a splay domain shown in Fig. 2(a). The nucleated loop then self-propels with its $+1/2$ section leading and adopts a prolate shape, with greatest curvature at the points with $\pm 1/2$ profiles. Changing the type of seeded elastic distortion, Fig. 4(b), leads to essentially the same nucleation process, with the sites of nucleation being the regions of maximal bend and the defect loops created having the same structure.

Our results can provide the basis for the analysis and interpretation of three-dimensional active nematic liquid crystals. Especially, it is important to realize that defect lines and loops in three-dimensional active nematics can exhibit a full span of different local orientational profiles—of $\pm 1/2$ wedge, twist, and mixed type—which results in profoundly different local self-propulsion velocities, both in the directions perpendicular and along the defect loop segment. There are many natural directions for extension of our work, including a detailed comparison of topologically charged and uncharged loops [19], the coupling between loop geometry and active dynamics, biaxiality in defect cores [37], and defects in active cholesterics [38,39]. The significance of two-dimensional topological defects to biological systems such as cell cultures and tissues has been well-established in recent years [5–7]; active defect loops may provide similar insights to fully three-dimensional biological tissues, fluids, and processes.

J. B. was supported by a University of Warwick IAS Early Career Fellowship. S. Č., Ž. K., and M. R. acknowledge funding from Slovenian Research Agency (ARRS) under Contracts No. P1-0099, No. J1-9149, No. N1-0124, and No. L1-8135. M. R. and G. P. A. thank the Isaac Newton Institute for Mathematical Sciences for support during the program "The mathematical design of new materials" under EPSRC Grant No. EP/R014604/1. This work was also supported by a STSM grant from the COST Action EUTOPIA (Grant No. CA17139).

*miha.ravnik@fmf.uni-lj.si
†G.P.Alexander@warwick.ac.uk

[1] S. Ramaswamy, The mechanics and statistics of active matter, Annu. Rev. Condens. Matter Phys. **1**, 323 (2010).
[2] M. C. Marchetti, J. F. Joanny, S. Ramaswamy, T. B. Liverpool, J. Prost, M. Rao, and R. A. Simha, Hydrodynamics of soft active matter, Rev. Mod. Phys. **85**, 1143 (2013).
[3] A. Doostmohammadi, J. Ignés-Mullol, J. M. Yeomans, and F. Sagués, Active nematics, Nat. Commun. **9**, 3246 (2018).
[4] H. H. Wensink, J. Dunkel, S. Heidenreich, K. Drescher, R. E. Goldstein, H. Löwen, and J. M. Yeomans, Meso-scale turbulence in living fluids, Proc. Natl. Acad. Sci. U.S.A. **109**, 14308 (2012).
[5] G. Duclos, C. Erlenkämper, J. F. Joanny, and P. Silberzan, Topological defects in confined populations of spindle-shaped cells, Nat. Phys. **13**, 58 (2017).
[6] K. Kawaguchi, R. Kageyama, and M. Sano, Topological defects control collective dynamics in neural progenitor cell cultures, Nature (London) **545**, 327 (2017).
[7] T. B. Saw, A. Doostmohammadi, V. Nier, L. Kocgozlu, S. Thampi, Y. Toyama, P. Marcq, C. T. Lim, J. M. Yeomans, and B. Ladoux, Topological defects in epithelia govern cell death and extrusion, Nature (London) **544**, 212 (2017).
[8] T. Sanchez, D. T. N. Chen, S. J. DeCamp, M. Heymann, and Z. Dogic, Spontaneous motion in hierarchically assembled active matter, Nature (London) **491**, 431 (2012).
[9] F. C. Keber, E. Loiseau, T. Sanchez, S. J. DeCamp, L. Giomi, M. J. Bowick, M. C. Marchetti, Z. Dogic, and A. Bausch, Topology and dynamics of active nematic vesicles, Science **345**, 1135 (2014).
[10] L. Giomi, M. J. Bowick, P. Mishra, R. Sknepnek, and M. C. Marchetti, Defect dynamics in active nematics, Phil. Trans. R. Soc. A **372**, 20130365 (2014).
[11] L. M. Pismen, Dynamics of defects in an active nematic layer, Phys. Rev. E **88**, 050502(R) (2013).
[12] S. P. Thampi, R. Golestanian, and J. M. Yeomans, Vorticity, defects and correlations in active turbulence, Phil. Trans. R. Soc. A **372**, 20130366 (2014).
[13] S. Shankar, S. Ramaswamy, M. C. Marchetti, and M. J. Bowick, Defect Unbinding in Active Nematics, Phys. Rev. Lett. **121**, 108002 (2018).
[14] D. Cortese, J. Eggers, and T. B. Liverpool, Pair creation, motion, and annihilation of topological defects in two-dimensional nematic liquid crystals, Phys. Rev. E **97**, 022704 (2018).
[15] D. Khoromskaia and G. P. Alexander, Vortex formation and dynamics of defects in active nematic shells, New J. Phys. **19**, 103043 (2017).
[16] P. W. Ellis, D. J. G. Pearce, Y.-W. Chen, G. Goldsztein, L. Giomi, and A. Fernandez-Nieves, Curvature-induced defect unbinding and dynamics in active nematic toroids, Nat. Phys. **14**, 85 (2018).

[17] S. Henkes, M. C. Marchetti, and R. Sknepnek, Dynamical patterns in nematic active matter on a sphere, Phys. Rev. E **97**, 042605 (2018).
[18] T. N. Shendruk, K. Thijssen, J. M. Yeomans, and A. Doostmohammadi, Twist-induced crossover from two-dimensional to three-dimensional turbulence in active nematics, Phys. Rev. E **98**, 010601(R) (2018).
[19] S. Čopar, J. Aplinc, Ž. Kos, S. Žumer, and M. Ravnik, Topology of Three-Dimensional Active Nematic Turbulence Confined to Droplets, Phys. Rev. X **9**, 031051 (2019).
[20] G. Duclos *et al.*, Topological structure and dynamics of three dimensional active nematics, arXiv:1909.01381.
[21] G. P. Alexander, B. G. Chen, E. A. Matsumoto, and R. D. Kamien, Colloquium: Disclination loops, point defects, and all that in nematic liquid crystals, Rev. Mod. Phys. **84**, 497 (2012).
[22] S. Čopar and S. Žumer, Nematic Braids: Topological Invariants and Rewiring of Disclinations, Phys. Rev. Lett. **106**, 177801 (2011).
[23] T. Machon and G. P. Alexander, Global defect topology in nematic liquid crystals, Proc. R. Soc. A **472**, 20160265 (2016).
[24] J. Friedel and P. G. de Gennes, Boulces de disclinations dans les cristaux liquides, C. R. Acad. Sc. Paris B **268**, 257 (1969).
[25] S. Čopar, T. Porenta, and S. Žumer, Nematic disclinations as twisted ribbons, Phys. Rev. E **84**, 051702 (2011).
[26] S. Čopar and S. Žumer, Quaternions and hybrid nematic disclinations, Proc. R. Soc. A **469**, 20130204 (2013).
[27] R. Green, J. Toner, and V. Vitelli, Geometry of thresholdless active flow in nematic microfluidics, Phys. Rev. Fluids **2**, 104201 (2017).
[28] See Supplemental Material at http://link.aps.org/supplemental/10.1103/PhysRevLett.124.088001 for further details of calculations, numerical methods and data analysis.
[29] R. Voituriez, J. F. Joanny, and J. Prost, Spontaneous flow transition in active polar gels, Europhys. Lett. **70**, 404 (2005).
[30] D. Marenduzzo, E. Orlandini, M. E. Cates, and J. M. Yeomans, Steady-state hydrodynamic instabilities of active liquid crystals: Hybrid lattice Boltzmann simulations, Phys. Rev. E **76**, 031921 (2007).
[31] J. Binysh and G. P. Alexander, Maxwell's theory of solid angle and the construction of knotted fields, J. Phys. A **51**, 385202 (2018).
[32] G. P. Alexander, Topology in liquid crystal phases, in *The Role of Topology in Materials*, edited by S. Gupta and A. Saxena (Springer International Publishing AG, Cham, 2018).
[33] A. N. Beris and B. J. Edwards, *Thermodynamics of Flowing Systems with Internal Microstructure* (Oxford University Press, New York, 1994).
[34] D. Seč, S. Čopar, and S. Žumer, Topological zoo of free-standing knots in confined chiral nematic fluids, Nat. Commun. **5**, 3057 (2014).
[35] S. Čopar, Topology and geometry of nematic braids, Phys. Rep. **538**, 1 (2014).
[36] S. P. Thampi, R. Golestanian, and J. M. Yeomans, Instabilities and topological defects in active nematics, Europhys. Lett. **105**, 18001 (2014).
[37] Ž. Krajnik, Ž. Kos, and M. Ravnik, Spectral energy analysis of bulk three-dimensional active nematic turbulence, arXiv:1912.09680.
[38] C. A. Whitfield, T. C. Adhyapak, A. Tiribocchi, G. P. Alexander, D. Marenduzzo, and S. Ramaswamy, Hydrodynamic instabilities in active cholesteric liquid crystals, Eur. Phys. J. E **40**, 50 (2017).
[39] L. Metselaar, A. Doostmohammadi, and J. M. Yeomans, Topological states in chiral active matter: Dynamic blue phases and active half-skyrmions, J. Chem. Phys. **150**, 064909 (2019).